PSI-SR-1211

Efficient, tunable near-infrared solid-state dye laser with good beam quality

Jeffrey A. Russell
Dennis P. Pacheco
Henry R. Aldag

Jeffrey A. Russell, Dennis P. Pacheco, Henry R. Aldag, "Efficient, tunable near-infrared solid-state dye laser with good beam quality ," presented at SPIE Photonics West (San Jose, CA), *Solid State Lasers XIV* **5707** (January2005).

Efficient, tunable near-infrared solid-state dye laser with good beam quality

Jeffrey A. Russell[†], Dennis P. Pacheco, and Henry R. Aldag
Physical Sciences Inc., 20 New England Business Center, Andover, MA, USA 01810-1077

ABSTRACT

We have demonstrated a laser-pumped, near-infrared solid-state dye laser (SSDL) with a slope efficiency ≅35%, tunability over ≅40 nm (from 710 to 750 nm) and $M^2 < 1.3$. This device utilizes a folded three-mirror resonator containing a tight focus for the gain medium and a collimated section for the tuning element. The folded cavity is astigmatically compensated through proper choice of sample thickness and cavity fold angle. We achieved low-threshold operation through the tight intracavity focus and by mounting the sample at Brewster's angle. Two pump lasers were used in this study: (1.) a flashlamp-pumped dye laser (FPDL) with an output wavelength of 630 nm and a pulse duration of ≅1 μs; and (2.) a pulsed red diode laser with an output wavelength of 671 nm and a pulse duration of ≅200 ns. The gain medium consists of the near-infrared dye Oxazine 725 in the solid host modified PMMA. With the FPDL as the pump source, slope efficiencies up to ≅35% were measured at the center of the tuning range. A single-plate birefringent filter (BRF) was used to tune the output from ≅710 to 750 nm with a single output wavelength. The BRF narrowed the spectral output from ≅15 to ≅0.8 nm, and provided smooth, continuous tuning over the 40-nm range. Lasing was observed outside this range, but the output consisted of two wavelengths separated by ≅50 nm (the free spectral range of the BRF). Time-resolved data showed that, for these cases, the laser switches from the shorter to the longer wavelength during the pulse. Input/output curves were generated as a function of resonator feedback for several output wavelengths. Findlay-Clay analyses were used to determine the round-trip cavity loss at each wavelength. The results correlate well with known losses in the resonator, including dye self-absorption losses. Beam-quality measurements were made near the peak of the tuning curve ($\lambda \cong 727$ nm) with a cavity feedback of 95%. At 1.5x threshold, the laser output had an M^2 value of ≅1.06. At 7x threshold, the beam quality degraded slightly to M^2 ≅1.26. Good temporal tracking was observed between the pump and output pulses, once the SSDL turned on. With design improvements to reduce the threshold, the tunable SSDL was also lased using the diode laser as the pump source. Further characterization of this device under direct diode-pumping is in process.

Keywords: Solid-state dye laser, diode-pumped, tunable, birefringent filter, beam quality, Oxazine 725 and modified PMMA

1. INTRODUCTION

Solid-state dye lasers pumped directly by diode lasers show great promise for the development of compact, efficient, inexpensive, tunable laser sources. The pulsed diode lasers themselves can be powered by commercially available rechargeable batteries, so the overall device is amenable to compact packaging and autonomous operation. Numerous military applications, including wavelength-agile communications, and medical applications, such as those utilizing the near-IR biological window, would benefit from such a compact, tunable device.

In previous work, we have reported on the basic laser characteristics of an untuned diode-pumped SSDL.[1,2] Key results that we have achieved to date include: untuned output with high laser efficiency (>25%), rep rates up to 1 kHz (limited by the diode pump laser) and excellent beam quality (M^2 ≅1.25). Our benchmark for assessing SSDL performance consists of earlier work done on direct *CW* diode-pumping of *liquid* dye solutions.[3,4] In this paper, we extend the capabilities of this technology to include broad tunability while maintaining high efficiency and excellent beam quality. In this investigation, we continued our successful strategy of initially using a flashlamp-pumped dye laser (FPDL) as a

[†] jar@psicorp.com; phone: 1.978.738.8170; fax: 1.978.689.3232; http://www.psicorp.com

surrogate for the diode pump laser[1,2,5] until we were able to demonstrate the low laser thresholds required for direct diode-pumping, and then switching to the pulsed diode pump source.

The organization of the paper is as follows. In Section 2, we discuss the experimental details, including descriptions of the gain media and pump lasers used, as well as the design of the tunable resonator. Section 3 discusses the experimental results obtained with an initial tunable resonator design. We will present input/output (I/O) measurements, Findlay-Clay analyses, time-resolved results, beam quality measurements and wavelength tuning data. The performance of an improved lower-threshold SSDL will be detailed in Section 4. Finally, a summary and concluding remarks will be given in Section 5.

2. EXPERIMENTAL DETAILS

2.1 Solid-state gain media

The solid dye gain media used in this study consisted of the dye Oxazine 725 (Ox 725) in modified PMMA (MPMMA). Figure 1 shows the normalized absorption and emission spectra for this dye in MPMMA. Although the fluorescence quantum yield of Ox 725 is only ≅ 0.11 in EtOH,[6] it is about three times higher in MPMMA (η_F ≅ 0.30). This increase is not unusual in going to a solid matrix, where the dye is effectively rigidized.[7] Table 1 summarizes the basic characteristics of the samples used in this investigation. Sample PSIN-017 was made primarily for FPDL pumping (at 630 nm) and PSIN-029 primarily for diode pumping (at 671 nm). The distinction arises from the fact that the FPDL excites Ox 725 near its absorption peak, while the diode laser pumps the dye well into the absorption tail. Therefore, different dye concentrations are required to achieve similar absorbances.

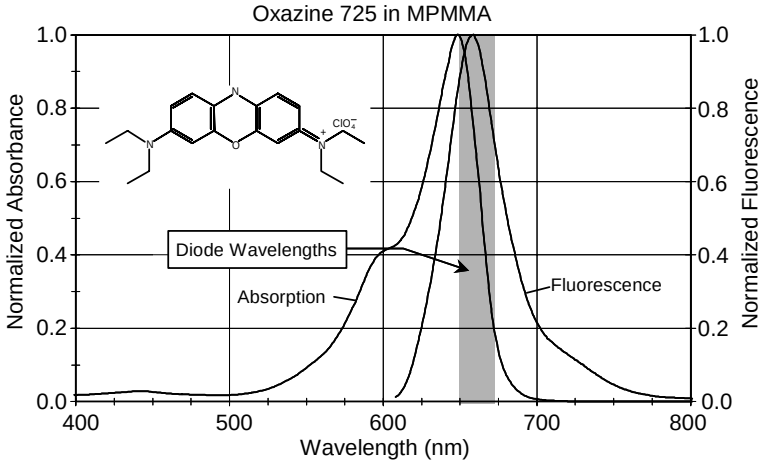

Figure 1: Normalized absorption and emission spectra of Ox 725 in MPMMA.

Table 1: Characteristics of the Solid Dye Gain Media Studied (Ox 725 in MPMMA)

Sample Designation	Dye Concentration (mM)	OD at 630 nm (FPDL)	OD at 671 nm (Diode Laser)
PSIN-017	1.0	≅3.5	≅1.3
PSIN-029	3.0	>5	>5

2.2 Pump lasers

Since red diode lasers are relatively low-power devices and a tunable resonator possesses a higher laser threshold than an untuned one, we performed the initial testing with the FPDL. We switched to the diode laser as the pump source once we developed the tunable SSDL cavity to a point where its threshold was below the pump levels attainable with the diode laser.

The FPDL can provide pulse energies of ≅60 mJ at 630 nm with a pulse duration of ≅1 μs (FWHM). The output of the FPDL was focused to a spot size comparable to that achievable with the red diode pump laser (≅80% of the energy transmitted through a 50-μm pinhole). The pump optics produced this spot size with an angle of incidence (θ_p in Figure 2) less than 4°. The 90° turning prism in the pump path was required in order to achieve this angle. Table 2 compares the output characteristics of the two pump lasers used in this study.

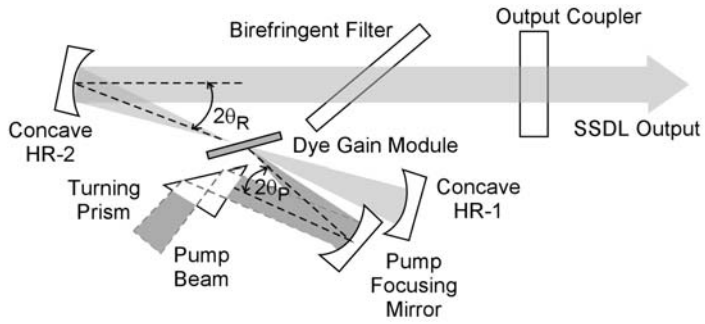

Figure 2: Resonator design for the tunable solid-state dye laser. The tuning element is the birefringent filter in the collimated section.

Table 2: Output Characteristics of the Pump Lasers Used in This Study

Parameter	Flashlamp-Pumped Dye Laser	Diode Laser
Energy / Pulse	>>1 mJ	≅1 μJ
Wavelength	≅630 nm	≅670 nm
Pulse Width	≅1 μs	≅0.2 μs (diode limitation)
Rep Rate	up to 10 Hz (typically 0.1 Hz)	up to 1 kHz (diode limitation)

2.3 Resonator design

Low-threshold dye lasers utilize an intracavity focus, where the resonator mode is highly concentrated. A small spot size is required when pumping with diode lasers, since they are relatively low-power devices. On the other hand, it is desirable to have a section of the cavity with low divergence for the placement of tuning elements. A resonator satisfying both requirements is shown in Figure 2. The design contains the requisite tight focus at the gain medium and a collimated section containing the tuning element, in this case a single-plate birefringent filter (BRF). The BRF was selected because: (1.) it is essentially lossless; (2.) it consumes very little space, and (3.) wavelength tuning is easily adapted to motorized control. This resonator has a decided advantage over our untuned design[1,2] in that it produces a nearly collimated output beam.

Mirrors for intracavity focusing are preferable to lenses, since mirror losses tend to be lower. The folded cavity, however, introduces astigmatic distortions. Furthermore, it is desirable to place the gain medium at Brewster's angle so as to minimize Fresnel losses, thereby lowering the laser threshold. The downside is that a gain medium oriented at Brewster's angle and placed at a small beam waist also introduces astigmatic distortions. Through proper choice of sample thickness, cavity fold angle and radius of curvature of HR-2, we were able to produce an astigmatically compensated cavity.[8]

For the initial tests, the optical layout of Figure 2 was assembled on a standard optical table. The experimental results for this configuration are detailed in Section 3.

2.4 Diagnostics for the SSDL output

Figure 3 shows the layout of the diagnostics for the SSDL output. The basic measurements include pulse energy, temporal profile, laser wavelength and bandwidth. The temporal profile of the SSDL output was displayed on an oscilloscope along with that of the pump beam for purposes of comparison. The Optical Multichannel Analyzer (OMA) records the laser output as a function of wavelength.

In order to successfully demonstrate a tunable diode-pumped SSDL, we must minimize the laser threshold. Since the lowest-order modes have the lowest thresholds, it is crucial to simultaneously optimize the beam quality (i.e., M^2) of the tunable SSDL. The procedures used to measure M^2 are described in Section 3.3.

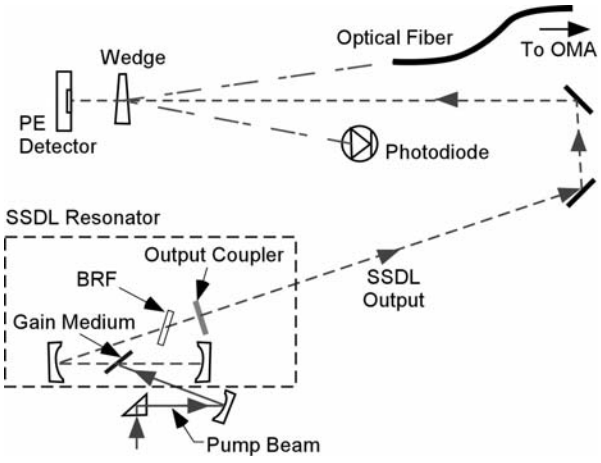

Figure 3: The optical layout of the diagnostics for the SSDL output.

2.5 Characterization of the birefringent filter (BRF)

Dye lasers have broad gain bandwidths, with values ranging from ≅25 to 75 nm, depending on the specific dye and resonator used. The BRF tuner is placed at Brewster's angle in the cavity and rotated about its axis of symmetry in order

to select the wavelength. (The axis of rotation for tuning the laser is perpendicular to the surface of the BRF. The axis for setting the BRF at Brewster's angle in the cavity is perpendicular to the plane of Figure 2.)

Numerous groups[9,10,11] have studied and modeled the BRF and its effect on the laser output wavelength. We used the work of Wang and Yao[9] to construct a MathCAD model to simulate the performance. In order to anchor the mathematical model, we measured the transmission of the BRF as a function of tuning angle for a fixed input wavelength. The experimental layout is shown in Figure 4. The BRF is mounted in an assembly which allows fine rotation in the plane of the filter. A HeNe laser (633 nm) was passed through a thin-sheet polarizer to produce a beam whose polarization is parallel to the optical table. A second polarizer installed after the BRF was set to pass light of the same polarization. The light transmitted through the second polarizer was then directed to a power meter. Transmitted power as a function of BRF tuning angle was then recorded.

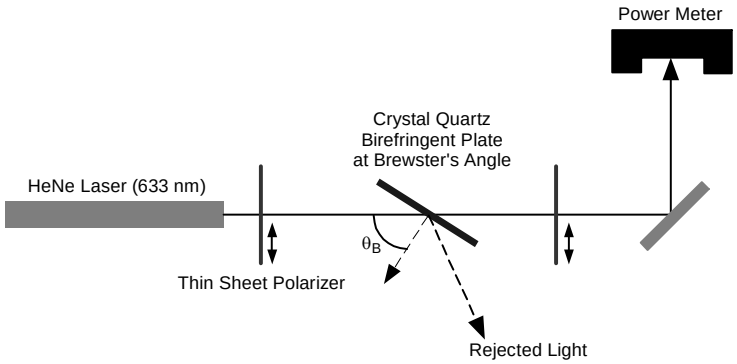

Figure 4: Experimental layout for measuring the transmission of the BRF tuner. (The black arrows indicate the polarization direction that is passed.) The BRF is rotated about its axis of symmetry, and the transmitted light is recorded as a function of this angle.

A BRF with a nominal thickness of 1 mm was chosen for the test, since it has a tuning range of ≅50 nm (which is approximately the tuning range of a typical dye). The actual thickness of the BRF was measured to be 1.028 mm. Figure 5 displays the experimental results together with the calculations of the MathCAD model. In order to cover the entire angular range, it was necessary to move the arm controlling the tuning angle to three different positions. (These are the various ranges indicated in the figure.) The optimum angular positions for wavelength-tuning lie near the middle of the curve (between 30° and 60°), because of the large rejection ratios observed. The model and the data are in excellent agreement in this region. The agreement is mediocre at the extremes of the angular range (ϕ < 20° and >70°). Since little phase retardation occurs near these extremes, this is not a region that is useful for tuning.

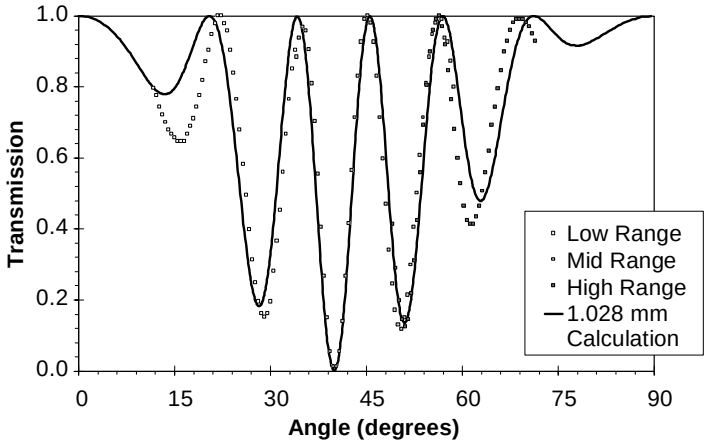

Figure 5: Comparison of experimental results and calculation for the transmission of polarized 633-nm light through the crystal quartz BRF. The agreement is excellent over the central (30° to 60°) region of the curve that is useful for tuning.

We next investigated the impact of small errors in setting the BRF at Brewster's angle. The "low range" of angles in Figure 5 was chosen for these measurements because of the larger deviation from the calculated values. The results are plotted on an expanded scale in Figure 6. While misalignment away from Brewster's angle tends to move the measured transmission closer to the calculated values, errors in excess of 3° are required for them to come into agreement. The accuracy of the alignment of the BRF to Brewster's angle is typically less than a degree, thereby excluding this as a possible explanation for the observed disagreement with the model. The impact of misalignment away from Brewster's angle also appears to most greatly affect the location of the minimum near ϕ = 15°, with that feature shifting a total of ≅1.5° (*versus* a shift of only ≅0.5° for the minimum near 30º). Overall, small misalignment of the BRF away from Brewster's angle will therefore have very little effect on the tuning capabilities of the single-plate BRF.

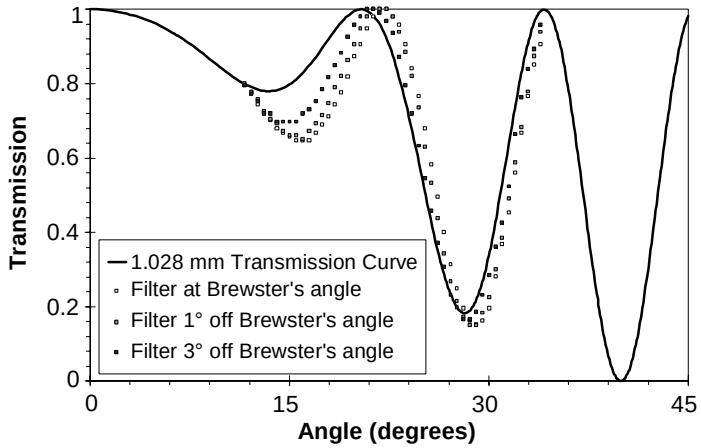

Figure 6: Effect on the BRF transmission curve as the angle of incidence is adjusted away from Brewster's angle. The effect is small except for angles below 20°. The best angles for laser tuning are in the range of 30° to 60°, because of the high rejection ratios.

3. LASER RESULTS AND ANALYSIS FOR THE INITIAL TUNABLE SSDL DESIGN

All measurements described in this section were made using sample PSIN-017 (Table 1) and the three-mirror resonator (Figure 2). The components were installed on a standard optical table using conventional mounts. Alignment and cavity-mirror spacing are critical in lowering the laser threshold to levels accessible to direct diode pumping.

Preliminary results were recorded with an untuned cavity (i.e., with the BRF absent), which allows us to obtain benchmark data for the three-mirror design. The untuned resonator, however, automatically selects the wavelength with the lowest threshold. This could lead to wavelength variations within a given set of data, complicating interpretation of the results. With the BRF installed in the cavity, the SSDL is kept at a particular wavelength throughout a set of experiments, simplifying the analysis.

3.1 Laser I/O curves

For this series of measurements, the SSDL was tuned to the middle of its range (≅727 nm) and output energy was recorded as a function of pump energy for several output couplers (Figure 7). As expected, the laser threshold decreases with increasing output-coupler reflectivity. This is because higher feedback results in higher intracavity flux, a higher rate of stimulated emission, and therefore a lower laser threshold. With the FPDL producing ≅1-μs pump pulses, the lowest observed threshold of 4.3 μJ (for R_{OC} = 98.5%) corresponds to ≅4.3 W of peak power. Pulsed red diode lasers are currently limited to ≅3 W of peak power, so further reduction in threshold was necessary before we could achieve lasing using a single diode pump laser (see Section 4.3). The highest slope efficiency measured in this series of tests is ≅35% (for R = 82.3%).

The round-trip cavity loss for the tuned resonator can be calculated from the I/O data using a Findlay-Clay analysis.[12] In this technique, the laser thresholds ($E_{threshold}$) are plotted against $-\ln(R_{OC})$, where R_{OC} is the reflectivity of the output coupler (Figure 8). The data are expected to follow the relation:

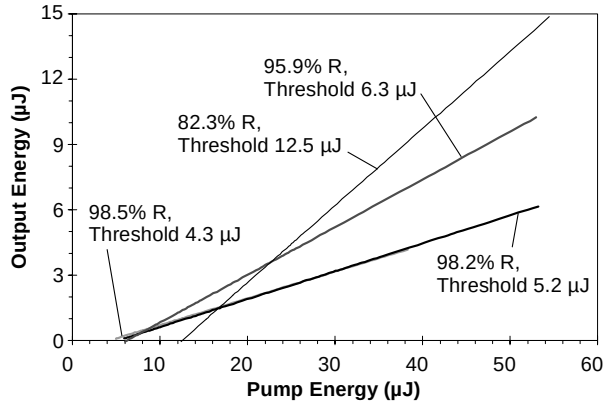

Figure 7: Energy I/O curves for the tuned resonator (λ ≅ 727 nm) for several output couplers. The legend identifies the output-coupler reflectivity for each data set and also reports the laser threshold. The actual data points are omitted for clarity. The sample is PSIN-017.

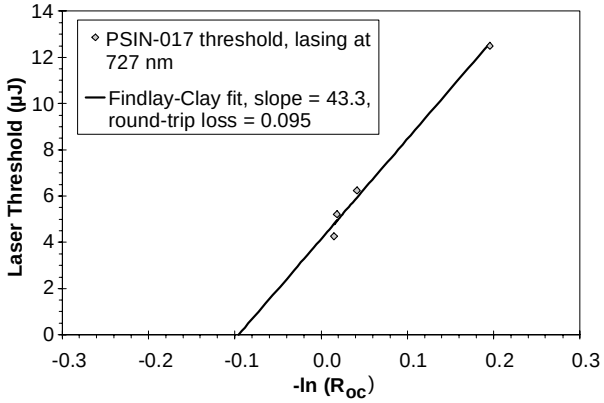

Figure 8: Findlay-Clay analysis for sample PSIN-017 tuned to 727 nm in three-mirror resonator.

$$E_{threshold} = K \cdot \left[-\ln(R_{OC}) + L \right], \quad (1)$$

where K is related to the round-trip gain and L is the round-trip loss in the cavity. A plot of $E_{threshold}$ versus $-\ln(R_{OC})$, therefore, should yield a straight line whose x-intercept is the round-trip loss L. From this analysis, the round-trip cavity loss was found to be 0.09, or about 9%, from the data of Figure 7.

The SSDL was then tuned to several other wavelengths (705, 716 and 750 nm) and the output energy again recorded as a function of pump energy for different output couplers. The laser threshold was determined as a function of output coupler for each wavelength and Findlay-Clay plots were generated (Figure 9). The primary observation is that the round-trip cavity loss is nearly identical for λ = 727 and 750 nm, and then increases as the laser wavelength decreases. This trend can be attributed to changes in dye self-absorption. That is, the absorption of the dye is essentially nil far out into the tail, and then increases as the wavelength decreases toward the absorption peak of ≅650 nm.

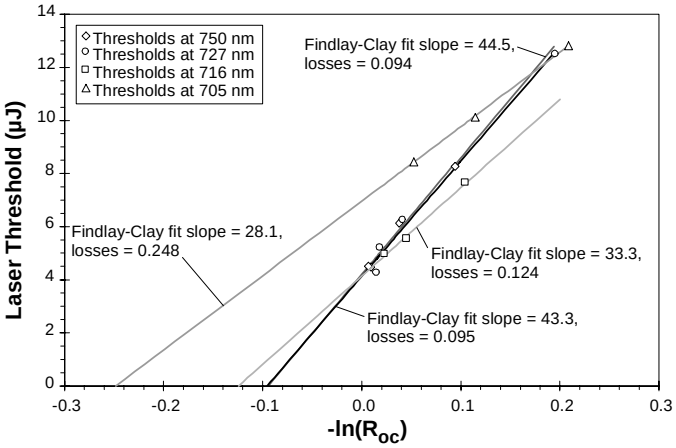

Figure 9: Findlay-Clay analyses for sample PSIN-017 in the three-mirror resonator at four wavelengths: 705, 716, 727 and 750 nm. The round-trip cavity loss increases as the output wavelength is tuned towards the peak absorption of the dye (≅650 nm).

3.2 Temporal behavior

Good temporal tracking between the pump and output pulses is required for efficient laser operation. Premature termination of the output pulse on a microsecond time scale can usually be ascribed to either thermooptical distortions in the solid gain medium or triplet-triplet absorption in the dye. In the present case, we observed very good temporal tracking for the SSDL over a wavelength range of ≅40 nm (from ≅710 to ≅750 nm) once the SSDL turns on (Figure 10). The time delay in the output pulse is due to mode build-up time in the cavity. A single output wavelength is observed in this spectral region.

The behavior is very different, however, when the laser is tuned outside of this range. As seen in Figure 11, the output pulse has a dip near the center. As the BRF is tuned slightly, the position of this dip moves across the pulse. By inserting a prism in the beam path to disperse the light and using a razor blade to block one of the two beams from reaching the photodiode, the temporal output can be resolved into two components at different wavelengths. Furthermore, by placing a 730-nm high-pass filter in the beam path, we were able to identify the

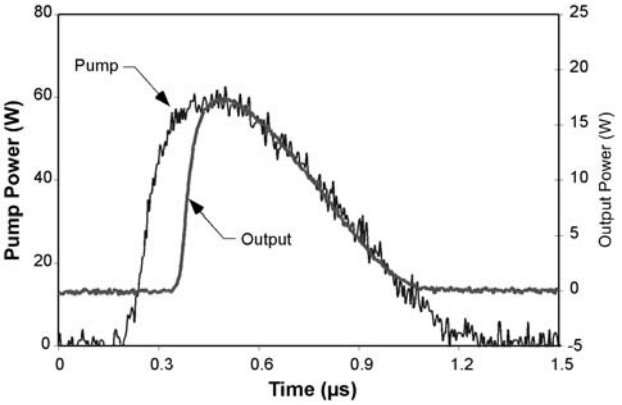

Figure 10: Very good temporal tracking is observed between the pump and output pulse over a tuning range from ≅710 to ≅750 nm. A single output wavelength is observed in this spectral region.

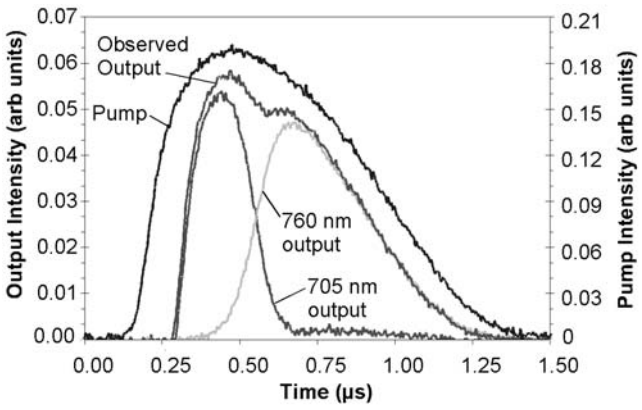

Figure 11: Temporal traces showing the pump profile (left axis) and the output profiles (right axis) for tuning at the extremes of the wavelength range. The observed output was resolved into two components at different wavelengths.

component appearing later in the pulse as the one possessing the longer wavelength. Using a monochromator, we measured the two wavelengths to be 705 and 760 nm. This dual-wavelength behavior is only observed at the extremes of the tuning range, and is thus easy to control by using a slightly thinner BRF (to increase its free spectral range) or else a different coating on the output coupler.

3.3 Beam quality measurements

The beam quality of the output is determined largely by the overlap of the resonator mode with the pumped volume in the gain medium. The spacing of the three resonator mirrors determines the minimum TEM_{00} mode size in the cavity. The pump mirror focal length and the placement of the gain medium with respect to both the cavity and pump-beam waists determine the actual beam waist of the SSDL.

We measured the beam quality (i.e., M^2) of the SSDL output for the three-mirror cavity tuned to 727 nm. For this set of measurements, we used a 95% R output coupler and pumped the gain medium at ≅1.5x and ≅7x threshold. A 100-mm focal length lens was placed 330 mm from the output coupler to bring the beam to focus, and a Coho 480 camera was mounted on a rail along the beam path to measure the beam size in the vicinity of the waist. A Spiricon framegrabber and software package were used to collect the beam images and measure the beam diameters. The software package has several different means of measuring beam diameters. We selected the 90-10 knife-edge criterion, which is the ISO standard. To extract the M^2 value from these data, the relevant equations are:

$$D^2(z) = D_0^2 + \Theta^2 (z - z_0)^2 \tag{2}$$

$$M^2 = \frac{\pi D_0 \Theta}{4\lambda} \tag{3}$$

where D(z) is the beam diameter at location z along the beam path, D_0 is the beam diameter at the waist, Θ is the full-angle beam divergence, z_0 is the location of the waist and λ is the laser wavelength. A least-squares fit of the data (Figure 12) yielded values for D_0 and Θ. The beam quality M^2 was then calculated from Eq. (3) using these values plus the known output wavelength. Analysis of the data shows that the SSDL has an M^2 of ≅1.06 at 1.5x threshold and ≅1.26 at 7x threshold.

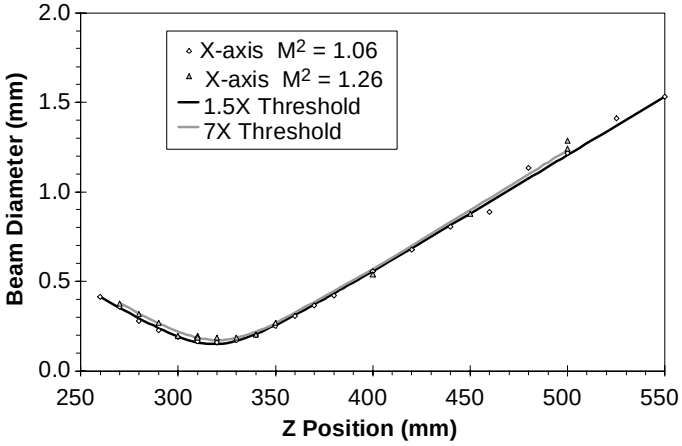

Figure 12: Beam quality measurements for the three-mirror SSDL. From these data, the M^2 value is ≅1.06 near threshold. When well above threshold, the M^2 value degrades slightly to ≅1.26.

3.4 Tuning range and laser bandwidth

The spectral output of the SSDL as a function of BRF tuning angle is shown in Figure 13. The data were taken in ~1° steps. As indicated earlier, the laser is tunable over ≅710 - 750 nm with a single output wavelength. The laser bandwidth in this range is ≅0.8 nm (FWHM), which is more than 10x narrower than the 15 nm measured with no BRF in the cavity. The transmission spectrum of the BRF has peaks separated by ≅60 nm. When the laser is tuned away from the peak of the gain, there is a point where the net round-trip gain (a combination of dye gain per pass, BRF transmission, mirror reflectivity and losses) is the same at two wavelengths simultaneously. At this point, the laser can oscillate at both wavelengths. This was shown earlier in Figure 11, where we observed that the laser initially runs at 705 nm, then switches to 760 nm (after ≅200 ns), where it remains for the duration of the pulse.

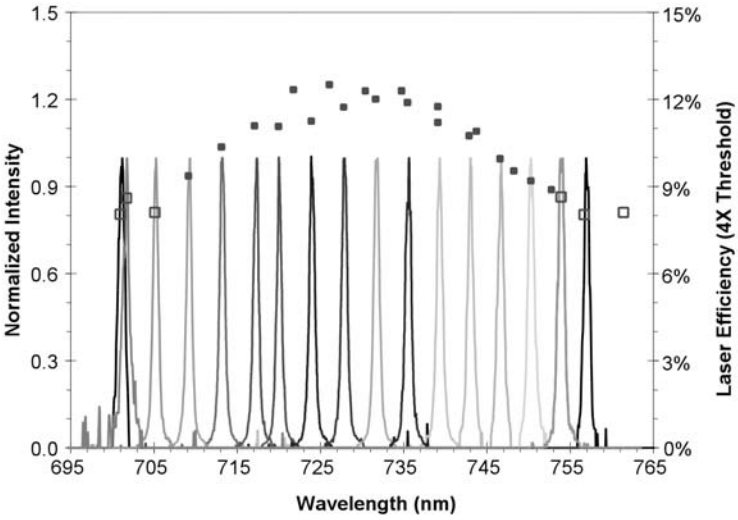

Figure 13: Normalized spectral data collected using a BRF in the three-mirror resonator of Figure 2. The peaks are separated by ≅3.7 nm, and each peak has a FWHM of ≅0.8 nm. The squares are laser efficiency data taken at 4x threshold and plotted on the right-hand axis. The efficiencies recorded at points where two output wavelengths were observed are displayed as open squares.

4. LASER RESULTS AND ANALYSIS FOR THE IMPROVED, LOWER-THRESHOLD TUNABLE SSDL

The initial optical layout (Figure 2) was redesigned in order to lower the threshold of the tunable SSDL to a level attainable with a single diode pump laser. This was achieved by reducing the TEM_{00} mode size in the gain medium and the pump spot size. The former involved reducing the radius of curvature of the HR-2 fold mirror and shortening the cavity. This resulted in a factor-of-two reduction in the mode volume. Shortening the cavity has the added advantage of reducing the mode build-up time, which increases the laser efficiency.

In order to facilitate positioning the optics to the required tolerances, we assembled the redesigned cavity on a single aluminum plate using custom mounts positioned to standard machining tolerances. For convenience in the following discussions, we will refer to this device as the "brassboard laser". Once we began diode pumping, the diode laser and associated pump optics were mounted to this plate as well.

The initial characterization of the brassboard laser was done using sample PSIN-017 as the gain medium and the FPDL as the pump source (Tables 1 and 2, respectively). The reflectivity of the output coupler (R_{OC}) was 98% and the SSDL was tuned to 725 nm. This relatively high feedback was selected in order to achieve a low laser threshold (at the expense of slope efficiency) for subsequent diode-pumping.

4.1 I/O measurements for the brassboard laser

Time-averaged I/O results are shown in Figure 14, with the fitting parameters shown in the inset. Since the pulse duration of the FPDL is ≅1 μs, the measured threshold of ≅2 μJ corresponds to a peak power of ≅2 W. This is now lower than the ≅3 W obtainable from a single pulsed red diode; thus, we can now achieve lasing under direct diode-pumping (Section 4.3). The output beam profile is also included in Figure 14, and is approximately Gaussian. (Detailed M^2 measurements were made and are presented in Section 4.2.)

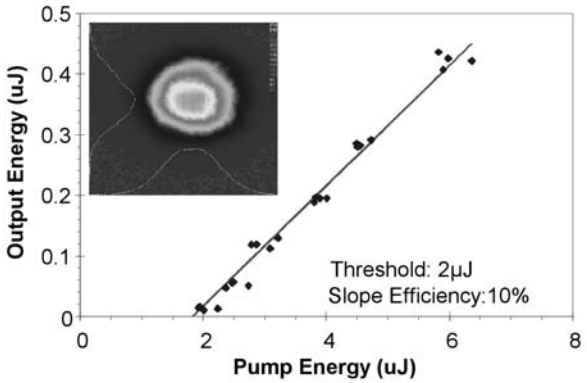

Figure 14: I/O curve for the brassboard solid-state dye laser with R_{OC} = 98% and the output tuned to 725 nm.

Time-resolved I/O data were also taken and are shown in Figure 15. The results confirm the pulse-averaged (i.e., energy) measurements. That is, the threshold intensity for the SSDL is ≅2W. The time-resolved data reveal that the laser threshold is more or less constant over the duration of the 1-μs pump pulse. The slope efficiency, however, decreases over this same time frame. Fortunately, the efficiency does not change much over the first 200 ns, which is the maximum pulse duration that we can use for the diode laser (Table 2).

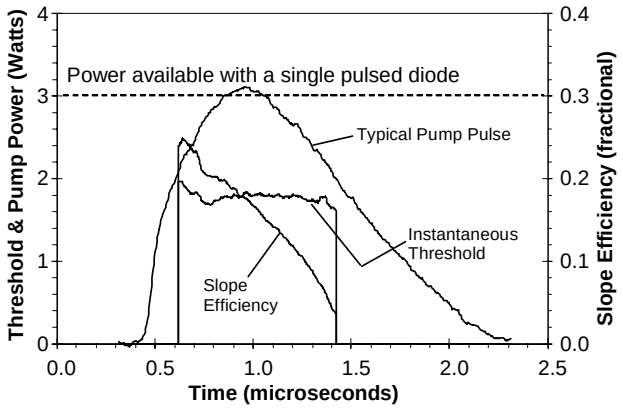

Figure 15: Time-resolved I/O data for the brassboard solid-state dye laser with R_{OC} = 98% and the output tuned to 725 nm. The threshold power is constant at ≅2W during the pulse. This is *below* the peak power available from the pulsed diode laser.

4.3 Direct diode-pumping of the tunable brassboard SSDL

The I/O results of Section 4.1, which were obtained with the FPDL, predict that we should be able to directly pump the tunable SSDL with a pulsed diode laser. This was confirmed by substituting the diode laser as the pump source in the brassboard device. The only other change made in the set-up was the use of sample PSIN-029 as the gain medium (Table 1). This was done to maximize the absorption of the diode pump light in single-pass. (Recall that the wavelength of the diode laser is ≅40 nm longer than that for the FPDL, and excites the dye in the long-wavelength tail.)

An unoptimized I/O curve for the diode-pumped tunable SSDL (R_{OC} = 98%) is shown in Figure 17. The laser was operated at ≅730 nm, which is near the peak of the tuning curve. The best fit to the data yield an energy threshold of ≅400 nJ and a slope efficiency of ≅5%. Since the pulse duration of the diode pump source is ≅200 ns, this energy threshold translates to a power threshold of ~2 W. This is consistent with the data obtained under dye laser pumping (Figures 14 and 15). Representative temporal traces are shown in the inset of Figure 17. These show that the SSDL output turns on relatively late in the diode current pulse (at t ≅ 100 ns), but this is expected to improve as the system is optimized. Further characterization is in process, including beam quality measurements and tuning curves.

4.2 Beam quality measurements for the brassboard laser

M^2 measurements were made as described previously in Section 3.3. The results are shown in Figure 16 for a pump intensity ≅ 3 – 4x threshold. The output is slightly astigmatic, which might be correctable with slight adjustments in the astigmatic compensation. The overall M^2 value of ≅1.2 indicates that the output beam is nearly diffraction-limited.

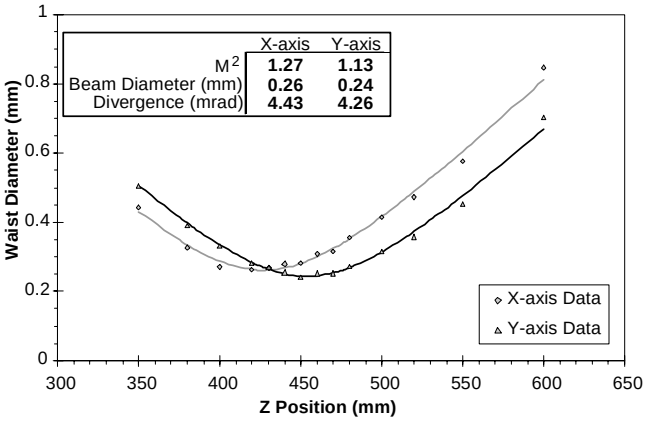

Figure 16: Beam quality measurements for the brassboard SSDL operated at ≅3 – 4x threshold. The values yielding the best fit for each data set are shown in the inset.

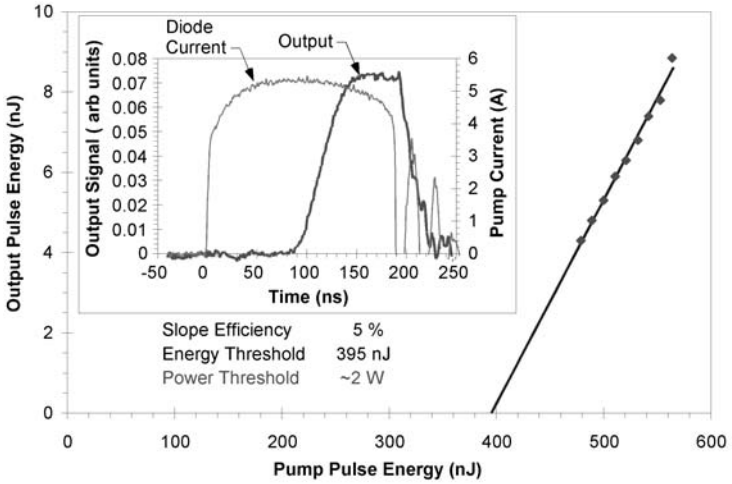

Figure 17: Unoptimized input/output curve for the brassboard diode-pumped tunable SSDL (R_{OC} = 98%). Typical temporal profiles for the diode current pulse and SSDL output are shown in the inset. The gain medium is Ox 725 (3 mM) in MPMMA.

5. CONCLUDING REMARKS

In summary, we have successfully demonstrated an efficient, tunable solid-state dye laser (SSDL) pumped directly by a diode laser. The gain medium consists of the near-IR dye Ox 725 in the solid host modified PMMA. Preliminary characterization of this SSDL was done using a flashlamp-pumped dye laser as the pump laser. With this excitation source, we have demonstrated slope efficiencies up to 35%. Using a single-plate birefringent filter (BRF), we were able to tune the SSDL over ≅40 nm (from ≅710 to ≅750 nm) with a single output wavelength. With the BRF, the bandwidth of the laser output narrowed from the free-running value of ≅15 nm down to ≅0.8 nm. Dual-wavelength operation was observed at the extremes of the tuning range (λ < 710 nm and >750 nm). Time-resolved data showed that, in these cases, the output wavelength switches by more than 50 nm during the pulse. A thinner BRF would eliminate this, if tuning into the low-gain regions is desired. Further reductions in bandwidth can be achieved by adding etalons to the resonator. Excellent beam quality (M^2 < 1.3) was measured for pump energies up to 7x threshold. Good temporal tracking was observed between the SSDL output and the diode pump pulse, which is important in achieving high laser efficiencies. With design improvements to reduce the threshold, this tunable SSDL was also successfully lased under direct diode-pumping.

It is worth noting that the diode pump laser operates on rechargeable batteries, and can run continuously for tens of hours at 1 kHz between charges. The device is therefore amenable to compact packaging and autonomous operation. Further characterization of the diode-pumped, tunable SSDL is in process, including I/O curves, beam quality measurements and tuning characteristics. Continued development of this technology is expected to result in an efficient, compact, inexpensive, broadly tunable laser source for a variety of medical and military applications.

ACKNOWLEDGEMENTS

We would like to thank Dr. Richard Scheps for extensive technical discussions and early support of the work. We also acknowledge Dr. Richard Tilton, William Russell, Anthony Sofia and Michael Reilly for technical support at PSI. This work was supported by a contract with the Department of Defense.

REFERENCES

1. D. P. Pacheco, W. H. Russell, J. A. Russell, et al., "Characterization and performance of pulsed red diode lasers for pumping dye lasers," in *Solid State Lasers XII*, R. Scheps, ed., Proc. SPIE **4968**, 35-45 (2003).
2. D. P. Pacheco, W. H. Russell and H. R. Aldag, "Solid-state dye lasers pumped directly by diode lasers," in *Solid State Lasers XIII*, R. Scheps and H. J. Hoffman, eds., Proc. SPIE **5332**, 180-188 (2004).
3. R. Scheps, "Near-IR dye laser for diode-pumped operation," IEEE J. Quantum Electron. **31**, 126 (1995).
4. R. Scheps, "Laser diode-pumped dye laser," in *UV and Visible Lasers and Laser Crystal Growth*, R. Scheps and M. Kokta, eds., Proc. SPIE **2380**, 274 (1995).
5. J. A. Russell, D. P. Pacheco, W. H. Russell, et al., "Laser threshold and efficiency measurements of solid-state dye lasers operating in the near-infrared under microsecond pumping," in *Solid State Lasers XI*, R. Scheps, ed., Proc. SPIE **4630**, 24-33 (2002).
6. R. Sens and K. Drexhage, "Fluorescence quantum yield of oxazine and carbazine laser dyes," J. Luminescence **24/25**, 709 (1981).
7. K. H. Drexhage, "Structure and Properties of Laser Dyes," in *Dye Lasers*, 3rd edition, F. P. Schafer, ed., Springer-Verlag, Berlin (1990), 158.
8. H. Kogelnik, E. P. Ippen, A. Dienes, and C. V. Shank, "Astigmatically compensated cavities for CW dye lasers," IEEE J. Quantum Electron. **QE-8**, 373 (1972).
9. X. Wang and J. Yao, "Transmitted and tuning characteristics of birefringent filters," Appl. Opt. **31**, 4505-4508 (1992).
10. D.R. Preuss and J.L. Gole, "Three-stage birefringent filter tuning smoothly over the visible region: theoretical treatment and experimental design," Appl. Opt. **19**, 702-710 (1980).
11. G. Holtam and O. Teschke, "Design of a birefringent filter for high-power dye lasers," IEEE J. Quantum Electron. **QE-10**, 577-579 (1974).
12. D. Findlay and R. A. Clay, "The measurement of internal losses in 4-level lasers", Phys. Lett. **20**, 277 (1966).